Technical Report

TR-01-32

Radiation effects in spent nuclear fuel canisters

Michael W Guinan

October 2001

Svensk Kärnbränslehantering AB
Swedish Nuclear Fuel
and Waste Management Co
Box 5864
SE-102 40 Stockholm Sweden
Tel 08-459 84 00
+46 8 459 84 00
Fax 08-661 57 19
+46 8 661 57 19

Radiation effects in spent nuclear fuel canisters

Michael W Guinan

October 2001

Summary

Calculations of neutron and gamma displacement damage rates for canisters of spent nuclear fuel have been done under contract to the Swedish Nuclear Fuel and Waste Management Company (SKB). For neutron and gamma spectra supplied by SKB for the spent fuel canisters, total defect production rates have been determined. The neutron damage code SPECTER (Argonne National Laboratory) and the Evaluated Photon Data Library (EPDL) coupled with the electron damage code DISP (Lawrence Livermore National Laboratory) were respectively used for the neutron and gamma damage calculations. By comparing with experiments in the literature, we were able to conclude that the magnitude of any physical property changes, e.g. yield stress, creep rates, enhanced solute segregation, dimensional changes, or brittleness, resulting from exposure over the service life of the of the canister will be negligible. Therefore, materials radiation effects will not impose any additional constraints on canister design.

Content

1 Introduction

The first step in evaluating radiation effects on materials is to determine the total defect production rate in the radiation spectrum of interest. Interaction cross-sections are used to determine the primary atomic recoil spectra which, when corrected for electronic energy losses, provide the damage energy spectra. Combined with experimental measurements of the minimum atomic displacement energy and damage efficiency as a function of recoil energy, the total defect production rate is determined.

Simple models of the displacement process predict that the number of displacements produced by an energetic recoil is proportional to the damage energy of the recoil. The total damage energy deposited per unit volume or per atom thus becomes a basis for comparing various irradiation experiments. It is customary however, to make comparisons on a displacements per atom (dpa) basis. For metals, a standard definition /1/ has been adopted based on the Kinchin-Pease model /2/. At high energies the number of displacements, <n> , produced by a recoil with damage energy E_D is given by

$$\langle n \rangle = 0.8\ E_D / 2E_A \qquad (1)$$

where E_A is the average displacement threshold, typically several tens of eV.

When experimental damage rates for fast and high energy neutrons are compared with those predicted by Equation (1), they are significantly lower than expected. In bcc metals the measured damage rates are about a factor of two lower than expected and in fcc metals a factor of three lower. On the other hand, damage rates measured in experiments for which recoil energies are in the range of 100 eV (e.g. using electrons or thermal neutrons) are in closer agreement with predicted values. In the standard model /1/ the factor 0.8 in Equation (1) is 1.0 for damage energies from 1 to 2.5 times the average threshold energy. Again, while it has been known for some time that fast neutrons are less efficient than electrons in producing damage, it is only in the last 5–10 years that quantitative comparisons could be made.

The accompanying Figures 1 and 2 compare experimental results for fcc copper /3/ and bcc iron /4/ from a variety of sources. The dashed lines in the figures correspond to Equation (1) while the solid lines are a fit to the data using an empirical relation proposed by Simons /5/. Dynamic computer simulations /6, 7/ reveal that the reduced production rates at high energies are due to a combination of cascade core melting and transport and recombination of ejected interstitials during cascade cooling. For a detailed discussion of displacement damage see the review article by Averback and de la Rubia /8/.

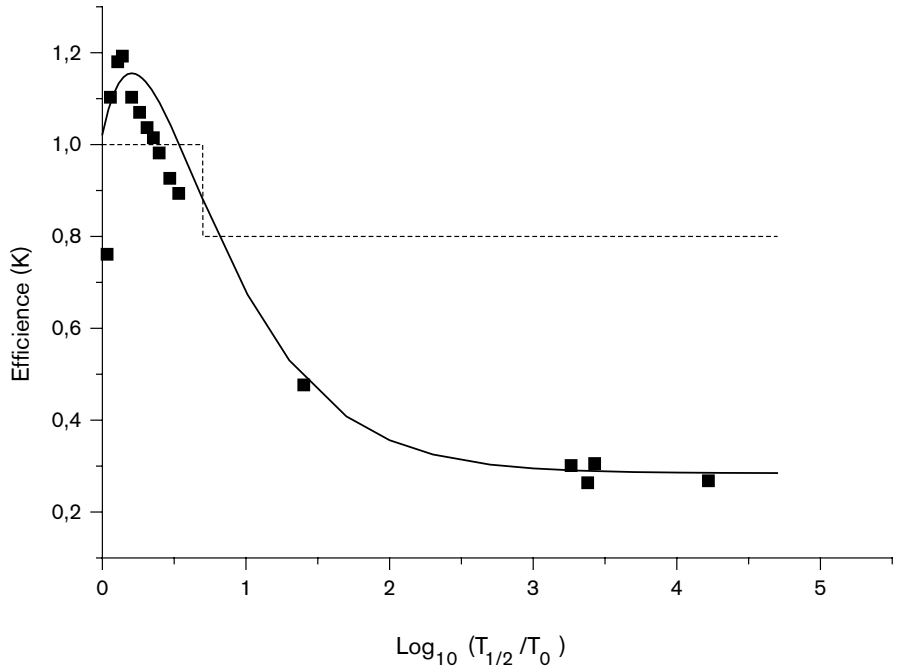

Figure 1. *Defect production efficiency in copper, K, inferred from resistivity changes at 4.2K for electrons and neutrons. K was calculated for T_0 = 19eV, Frenkel pair resistivity, ρ_f = 2.5 x 10^{-4} Ω-cm/dpa, and E_A= 40eV. $T_{1/2}$ is the recoil energy for each damage spectrum at which half the integrated damage, E_{DAM}, is reached. The dashed line is the standard (NRT) definition /1/ and the solid line is a fit to Simon's /5/ expression (k = 1.395ln(x)/x + 0.7376/x + 0.285, where $x = T_{1/2}/T_0$).*

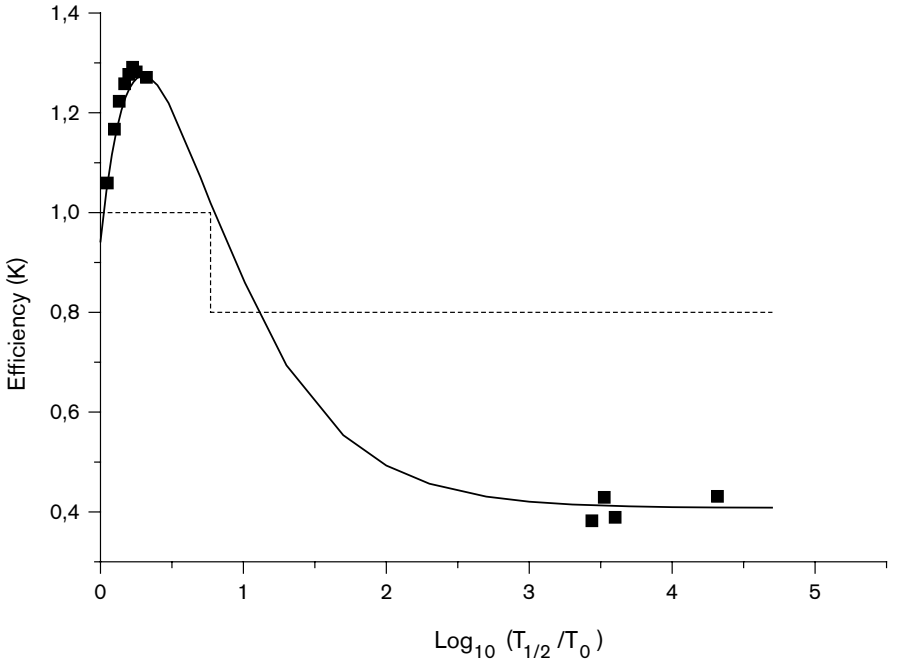

Figure 2. *Defect production efficiency in iron, K, inferred from resistivity changes at 4.2K for electrons and neutrons. K was calculated for T_0 = 17eV, Frenkel pair resistivity, ρ_f = 15 x 10^{-4} Ω-cm/dpa, and E_A= 40eV. $T_{1/2}$ is the recoil energy for each damage spectrum at which half the integrated damage, E_{DAM}, is reached. The dashed line is the standard (NRT) definition /1/ and the solid line is a fit to Simon's /5/ expression (k = 1.729ln(x)/x + 0.534/x + 0.408, where $x = T_{1/2}/T_0$).*

2 Calculations

In the following two sections displacement damage energy cross-sections are calculated for each of the 23 neutron groups and the 10 gamma discrete ordinances utilized by Håkansson /9/ in his report of neutron and gamma fluxes for various SKB canister configurations.

Neutron Damage Cross-Sections

The Argonne National Laboratory code, SPECTER /10/, was used to determine damage energy cross-sections for the 23 neutron groups by collapsing the 100 group cross section file of SPECTER. The version I had available used the ENDF/B-V data file /11/.

Calculations were made for both iron and copper. The canister configurations for BWR and PWR fuel assemblies used by Håkansson /9/ are shown in Figure 3. Calculation points, situated at the mid-plane of the fuel canisters, are indicated by the labels A and D. These correspond to the positions of highest fluxes around the circumference of the canisters. Fluxes at the iron-copper interfaces, labeled I, were interpolated using neutron attenuation coefficients for both metals. Håkansson determined fluxes for three BWR cases (40 and 45 MWd burn-ups after 30 years decay and 45 MWd after 40 years decay) and 3 PWR cases for 50 MWd burn-ups (3.5% and 4.0% enriched fuels after 30 years and 3.5% after 40 years decay).

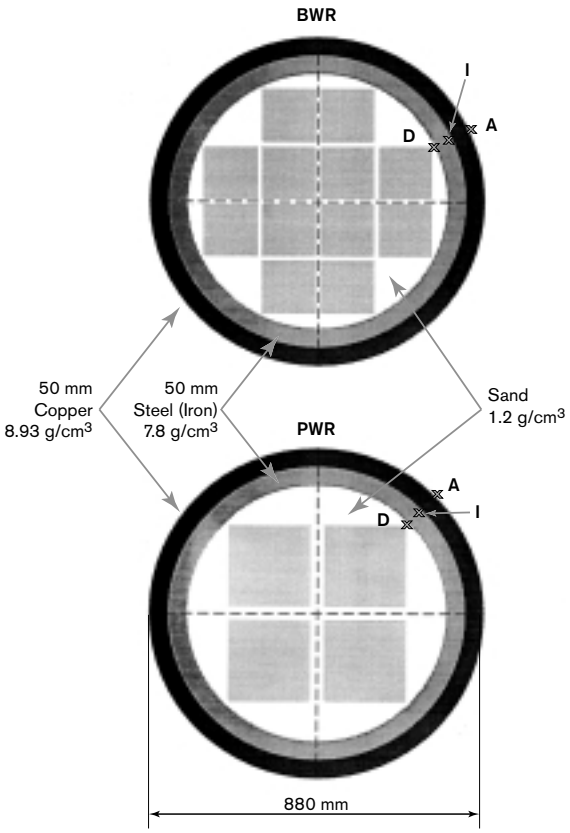

Figure 3. *The canister configuration for BWR and PWR fuel assemblies used by Håkansson /9/.*

Table 1 gives damage energy cross-sections, s_{DE}, for copper for each of the 23 neutron groups. Group bounds are listed as well as the fluxes for the six cases described above at positions A and I. At the bottom of each column the total flux and spectrum averaged damage energy cross-section are tabulated. We have also included the total damage energy deposition rate (flux times σ_{DE}) in units of 10^{-21} eV/s. Since, in reactor experiments, fluxes with E>0.1 MeV are generally reported as a measure of exposure, these are also tabulated with the corresponding damage energy cross-sections. For comparison, damage energy cross-sections for E>0.1 MeV are listed at the bottom of the table for U235 fission and three research reactor facilities (BSR at ORNL /12/, FRM at Munich /13/ and CP-5 at ANL /14/)and a D-T neutron source (RTNS-II at LLNL/15/). Table 2 Lists the same information for iron at positions I and D.

The current canister design /16/ shown in Figure 4 is slightly larger (1050 mm diameter instead of 880 mm diameter) and is completely filled with cast iron instead of sand plus a 50 mm steel shell. However, the copper shell thickness (50 mm) is the same in both cases as is the spacing between the nearest fuel assembly and the outer copper surface. As a result, we expect only minor differences in neutron fluxes. The results here are at most 10% larger than for the new design.

To put things in perspective, we note that while the fluxes at the canisters range from 1 to 6×10^{4} n/cm^{2}s, those in the research reactors range from 2 to 10×10^{12} n/cm^{2}s. This means that a one year neutron exposure to the spent fuel corresponds to ~ a one second neutron exposure in the research reactor facilities.

Gamma Damage Cross-Sections

The starting point for gamma damage calculations begins with the determination of electron damage energy cross sections, σ_{DE}. These were determined for both copper and iron from the minimum electron energy required to produce a displacement E_{min} (0.33

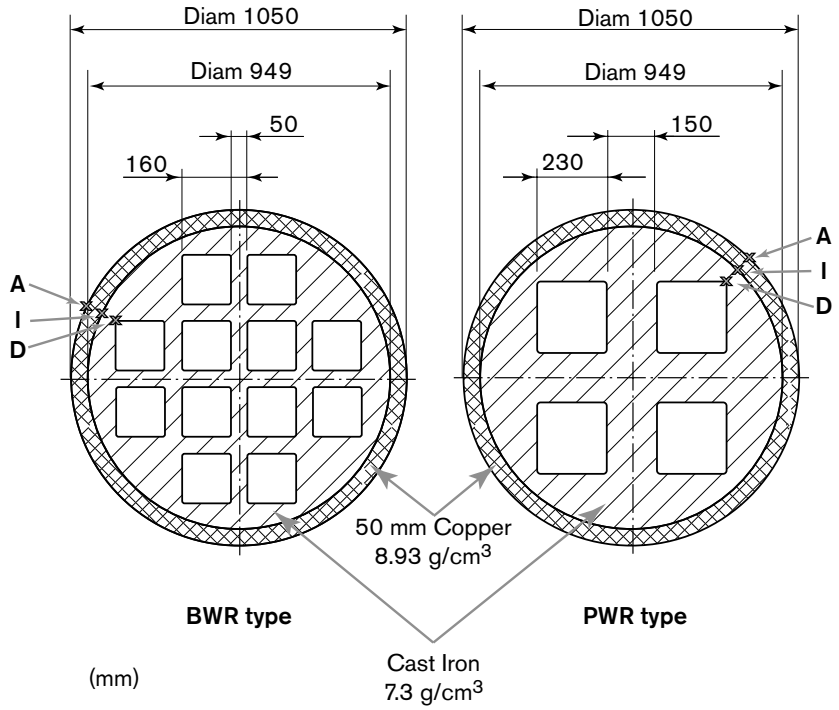

Figure 4. *The current canister design /16/.*

MeV for copper and 0.40 MeV for iron) to a maximum energy of 10 MeV. Since the electrons produced by gammas end up stopping in the material, for a given electron energy E_1 we need to integrate the cross section from that energy to the minimum energy for a displacement. The total damage energy for an electron of energy E_1 stopping in the material, E_{DAM} (E_1), is, therefore:

$$E_{DAM}(E_1) = (N/\rho)\int_{E_{\min}}^{E_1} K(E)(\sigma_{DE}(E)/S(E))dE \qquad (2)$$

where N/ρ is the number of atoms/gram, K(E) is the damage efficiency taken from Figures 1 and 2 for copper and iron, and S(E) is the electronic stopping power in MeVcm^2/g. The values for σ_{DE}(E) were calculated using the Livermore DISP code /17/ and S(E) was taken from the AIP Handbook /18/.

A gamma interacting with a material can produce recoil electrons through three different processes: (1) photoelectric absorption, (2) Compton scattering, and (3) pair production. For each of these processes, we integrated over the differential energy spectrum of electrons produced by a gamma of energy E_γ multiplied by the damage energy, E_{DAM}. This gives us the total damage produced by each of the interactions. When we multiply by the cross section for that interaction, we obtain the damage energy cross section for that process and energy. Summing over the three processes, we obtain the total damage energy cross section for gammas of energy E_γ..

The differential energy spectra for each of the processes were taken from Evans /19/ and the interaction cross sections from the LLNL Evaluated Photon Data Library /20/. The calculated damage energy cross sections are given in Table 3 for each of the discrete gamma energies used by Håkansson /9/ and for the relevant energy groups used by Lundgren /21/.

The corresponding γ-fluxes are given in /9/ for each of the six cases (3 PWR and 3 BWR) described for neutron damage. In these cases, results are only available at the surface of the canister (Position A). For the BWR Lundgren /21/ provides results for 38 MWd at 30 years decay for the dose rate in mSv/h for each group at positions A and D (Appendix 1). Since he also lists the response functions used for each group, we were able to convert to equivalent γ-fluxes. As before, fluxes at the iron-copper interface were interpolated from A and D.

For each of the cases in /9/, the total g-flux and corresponding spectrum averaged damage energy cross-sections are tabulated for copper at position A. As Table 3 shows, there is little variation in σ_{DE} with either burn-up or enrichment, but the cross-section at 40 years decay is only 2/3 the value at 30 years. For later reference, Table 3 also includes the total damage energy deposition rate (flux times σ_{DE}) in units of 10^{-21} eV/s.

For the 38 MWd case considered in /21/, the spectrum averaged σ_{DE} at position A is only 60% of that from /9/ at 40 MWd. This results from the higher (x2) flux in the lowest energy group (0.510–0.800 MeV). Lundgren /21/ attributes this primarily to the difference in the filling materials (sand vs. cast iron). However, the deposition rate is nearly the same since this group only contributes ~ 13% to this rate at 38 MWd /21/ and 3.5% at 40 MWd /9/.

For Cu, the flux at position I is 27 times that at A with a σ_{DE} of 62% that at A. For Fe the flux at D is 25 times that at I with a σ_{DE} of 75% that at I. This is consistent with the relative hardening of the spectra expected for 50 mm of cast iron or copper.

Table 1. Neutron Damage in Copper

Group Energy (MeV)		Group	PWR Group Flux @ Position I			PWR Group Flux @ Position A		
Upper	Lower	$\sigma_{\Delta E}$ (barn-keV)	3.5%@30y n/cm²s	4.0%@30y n/cm²s	3.5%@40y n/cm²s	3.5%@30y n/cm²s	4.0%@30y n/cm²s	3.5%@40y n/cm²s
1,000E+01	6,065E+	199,77	2,110E+02	1,661E+02	1,471E+02	1,145E+02	9,012E+01	7,982E+01
6,065E+00	3,679E+00	154,40	8,992E+02	7,080E+02	6,271E+02	4,728E+02	3,722E+02	3,297E+02
3,679E+00	2,231E+00	107,05	2,244E+03	1,767E+03	1,565E+03	1,241E+03	9,774E+02	8,656E+02
2,231E+00	1,353E+00	74,77	3,407E+03	2,683E+03	2,376E+03	1,986E+03	1,564E+03	1,385E+03
1,353E+00	8,210E-01	58,61	4,644E+03	3,656E+03	3,238E+03	2,810E+03	2,212E+03	1,960E+03
8,210E-01	5,000E-01	45,21	7,133E+03	5,611E+03	4,972E+03	4,251E+03	3,345E+03	2,964E+03
5,000E-01	1,110E-01	25,06	1,249E+04	9,828E+03	8,709E+03	6,984E+03	5,495E+03	4,869E+03
1,110E-01	9,118E-03	8,87	4,500E+03	3,524E+03	3,138E+03	1,766E+03	1,384E+03	1,231E+03
9,118E-03	5,530E-03	2,90	2,904E+02	2,270E+02	2,025E+02	9,144E+01	7,161E+01	6,375E+01
5,530E-03	1,487E-04	0,85	4,831E+02	3,766E+02	3,369E+02	2,333E+02	1,823E+02	1,626E+02
1,487E-04	1,597E-05	0,05	1,071E+02	8,264E+01	7,469E+01	3,457E+01	2,685E+01	2,410E+01
1,597E-05	9,877E-06	0,06	7,119E+00	5,457E+00	4,963E+00	3,547E+00	2,747E+00	2,473E+00
9,877E-06	4,000E-06	0,09	5,150E+00	3,951E+00	3,591E+00	2,599E+00	2,007E+00	1,812E+00
4,000E-06	1,855E-06	0,13	1,535E+00	1,182E+00	1,070E+00	7,286E-01	5,627E-01	5,080E-01
1,855E-06	1,097E-06	0,19	8,059E-01	6,218E-01	5,622E-01	4,500E-01	3,472E-01	3,137E-01
1,097E-06	1,020E-06	0,21	6,312E-02	4,870E-02	4,401E-02	4,258E-02	3,287E-02	2,969E-02
1,020E-06	6,250E-07	0,25	2,369E-01	1,825E-01	1,652E-01	1,405E-01	1,084E-01	9,794E-02
6,250E-07	3,500E-07	0,32	1,307E-01	1,002E-01	9,113E-02	7,738E-02	5,978E-02	5,396E-02
3,500E-07	2,800E-07	0,39	2,762E-02	2,119E-02	1,926E-02	1,817E-02	1,404E-02	1,267E-02
2,800E-07	1,400E-07	0,50	3,989E-02	3,060E-02	2,782E-02	2,478E-02	1,916E-02	1,728E-02
1,400E-07	5,800E-08	0,74	1,831E-02	1,399E-02	1,277E-02	1,260E-02	9,742E-03	8,783E-03
5,800E-08	3,000E-08	1,11	3,986E-03	3,040E-03	2,780E-03	2,877E-03	2,226E-03	2,005E-03
3,000E-08	1,000E-10	5,94	2,102E-03	1,605E-03	1,466E-03	1,405E-03	1,089E-03	9,796E-04
Total Flux (n/cm²s)			3,642E+04	2,864E+04	2,540E+04	1,999E+04	1,573E+04	1,394E+04
Spectrum $\sigma_{\Delta E}$ (barnkeV)			44,6	44,6	44,6	46,3	46,3	46,3
DE Rate (E-21 eV/s)			1,625E+06	1,279E+06	1,133E+06	9,252E+05	7,283E+05	6,452E+05
E>0.1MeV Flux (n/cm²s)			3,147E+04	2,477E+04	2,195E+04	1,804E+04	1,419E+04	1,258E+04
E>0.1MeV $\sigma_{\Delta E}$ (barnkeV)			51,6	51,6	51,6	51,3	51,3	51,3
Facility			235U fission spectrum			BSR		FRM
E>0.1MeV $\sigma_{\Delta E}$ (barnkeV)			79,2			77,3		68,9

Table 1. continue

BWR Group Flux @ Position I			BWR Group Flux @ Position A		
45MWd@30y n/cm²s	45MWd@40y n/cm²s	40MWd@30y n/cm²s	45MWd@30y n/cm²s	45MWd@40y n/cm²s	40MWd@30y n/cm²s
11,654E+02	1,154E+02	1,010E+02	7,823E+01	5,459E+01	4,778E+01
7,020E+02	4,898E+02	4,288E+02	3,243E+02	2,263E+02	1,981E+02
1,749E+03	1,220E+03	1,068E+03	8,634E+02	6,025E+02	5,274E+02
2,667E+03	1,861E+03	1,629E+03	1,420E+03	9,909E+02	8,674E+02
3,686E+03	2,572E+03	2,252E+03	2,042E+03	1,425E+03	1,248E+03
5,432E+03	3,790E+03	3,323E+03	3,017E+03	2,105E+03	1,846E+03
9,384E+03	6,546E+03	5,765E+03	4,952E+03	3,456E+03	3,043E+03
4,299E+03	3,000E+03	2,643E+03	1,578E+03	1,101E+03	9,697E+02
3,552E+02	2,478E+02	2,184E+02	8,702E+01	6,072E+01	5,352E+01
1,226E+03	8,551E+02	7,536E+02	3,402E+02	2,374E+02	2,091E+02
4,441E+02	3,098E+02	2,726E+02	9,424E+01	6,575E+01	5,788E+01
4,294E+01	2,997E+01	2,639E+01	1,236E+01	8,587E+00	7,590E+00
3,940E+01	2,750E+01	2,437E+01	1,178E+01	8,251E+00	7,254E+00
1,917E+01	1,338E+01	1,201E+01	4,209E+00	2,937E+00	2,608E+00
1,236E+01	8,626E+00	7,786E+00	3,281E+00	2,289E+00	2,043E+00
6,782E-01	4,733E-01	4,263E-01	3,231E-01	2,254E-01	2,014E-01
4,481E+00	3,127E+00	2,826E+00	1,153E+00	8,044E-01	7,201E-01
3,415E+00	2,383E+00	2,131E+00	6,873E-01	4,796E-01	4,292E-01
6,346E-01	4,428E-01	3,943E-01	1,630E-01	1,138E-01	1,017E-01
1,257E+00	8,772E-01	7,785E-01	2,096E-01	1,463E-01	1,304E-01
8,831E-01	6,160E-01	5,408E-01	9,935E-02	6,936E-02	6,167E-02
2,199E-01	1,534E-01	1,336E-01	1,940E-02	1,354E-02	1,202E-02
9,284E-02	6,476E-02	5,623E-02	6,940E-03	4,845E-03	4,276E-03
3,023E+04	2,110E+04	1,853E+04	1,483E+04	1,035E+04	9,089E+03
41,8	41,8	41,8	44,4	44,4	44,4
1,265E+06	8,827E+05	7,740E+05	6,590E+05	4,599E+05	4,032E+05
2,421E+04	1,689E+04	1,483E+04	1,285E+04	8,970E+03	7,875E+03
52,2	52,2	52,2	51,3	51,3	51,2
	CP-5		RTNS-II		
	56,3		296,0		

Table 2. Neutron Damage in Iron

Group Energy (MeV)		Group	PWR Group Flux @ Position D			PWR Group Flux @ Position I		
Upper	Lower	$\sigma_{\Delta E}$ (barn-keV)	3.5%@30y n/cm²s	4.0%@30y n/cm²s	3.5%@40y n/cm²s	3.5%@30y n/cm²s	4.0%@30y n/cm²s	3.5%@40y n/cm²s
1,000E+01	6,065E+00	205,99	3,964E+02	3,121E+02	2,764E+02	2,110E+02	1,661E+02	1,471E+02
6,065E+00	3,679E+00	166,83	1,801E+03	1,418E+03	1,256E+03	8,992E+02	7,080E+02	6,271E+02
3,679E+00	2,231E+00	124,03	4,457E+03	3,509E+03	3,108E+03	2,244E+03	1,767E+03	1,565E+03
2,231E+00	1,353E+00	82,59	6,182E+03	4,868E+03	4,311E+03	3,407E+03	2,683E+03	2,376E+03
1,353E+00	8,210E-01	51,76	7,237E+03	5,697E+03	5,046E+03	4,644E+03	3,656E+03	3,238E+03
8,210E-01	5,000E-01	41,26	1,144E+04	8,999E+03	7,975E+03	7,133E+03	5,611E+03	4,972E+03
5,000E-01	1,110E-01	24,86	2,222E+04	1,749E+04	1,550E+04	1,249E+04	9,828E+03	8,709E+03
1,110E-01	9,118E-03	7,52	9,944E+03	7,788E+03	6,934E+03	4,500E+03	3,524E+03	3,138E+03
9,118E-03	5,530E-03	2,63	8,282E+02	6,474E+02	5,776E+02	2,904E+02	2,270E+02	2,025E+02
5,530E-03	1,487E-04	0,35	6,519E+02	5,082E+02	4,546E+02	4,831E+02	3,766E+02	3,369E+02
1,487E-04	1,597E-05	0,02	1,683E+02	1,299E+02	1,174E+02	1,071E+02	8,264E+01	7,469E+01
1,597E-05	9,877E-06	0,05	1,272E+01	9,749E+00	8,867E+00	7,119E+00	5,457E+00	4,963E+00
9,877E-06	4,000E-06	0,07	8,768E+00	6,727E+00	6,114E+00	5,150E+00	3,951E+00	3,591E+00
4,000E-06	1,855E-06	0,10	2,723E+00	2,096E+00	1,899E+00	1,535E+00	1,182E+00	1,070E+00
1,855E-06	1,097E-06	0,14	1,238E+00	9,552E-01	8,636E-01	8,059E-01	6,218E-01	5,622E-01
1,097E-06	1,020E-06	0,16	8,488E-02	6,549E-02	5,919E-02	6,312E-02	4,870E-02	4,401E-02
1,020E-06	6,250E-07	0,18	3,451E-01	2,659E-01	2,406E-01	2,369E-01	1,825E-01	1,652E-01
6,250E-07	3,500E-07	0,24	1,936E-01	1,484E-01	1,350E-01	1,307E-01	1,002E-01	9,113E-02
3,500E-07	2,800E-07	0,29	3,772E-02	2,894E-02	2,630E-02	2,762E-02	2,119E-02	1,926E-02
2,800E-07	1,400E-07	0,36	5,621E-02	4,311E-02	3,920E-02	3,989E-02	3,060E-02	2,782E-02
1,400E-07	5,800E-08	0,54	2,405E-02	1,838E-02	1,677E-02	1,831E-02	1,399E-02	1,277E-02
5,800E-08	3,000E-08	0,81	5,056E-03	3,856E-03	3,526E-03	3,986E-03	3,040E-03	2,780E-03
3,000E-08	1,000E-10	4,41	2,835E-03	2,164E-03	1,977E-03	2,102E-03	1,605E-03	1,466E-03
Total Flux (n/cm²s)			6,535E+04	5,139E+04	4,557E+04	3,642E+04	2,864E+04	2,540E+04
Spectrum $\sigma_{\Delta E}$ (barnkeV)			44,7	44,8	44,7	44,8	44,9	44,8
DE Rate (E-21 eV/s)			2,922E+06	2,300E+06	2,037E+06	1,633E+06	1,285E+06	1,139E+06
E>0.1MeV Flux (n/cm²s)			5,473E+04	4,307E+04	3,817E+04	3,147E+04	2,477E+04	2,195E+04
E>0.1MeV $\sigma_{\Delta E}$ (barnkeV)			53,4	53,4	53,4	51,9	51,9	51,9
Facility			235U fission spectrum			BSR		FRM
E>0.1MeV $\sigma_{\Delta E}$ (barnkeV)			84,4			80,3		70,9

Table 2. continue

BWR Group Flux @ Position D			BWR Group Flux @ Position I		
45MWd@30y n/cm²s	45MWd@30y n/cm²s	45MWd@40y n/cm²s	45MWd@30y n/cm²s	45MWd@40y n/cm²s	40MWd@30y n/cm²s
3,107E+02	2,168E+02	1,898E+02	1,654E+02	1,154E+02	1,010E+02
1,406E+03	9,810E+02	8,589E+02	7,020E+02	4,898E+02	4,288E+02
3,473E+03	2,423E+03	2,121E+03	1,749E+03	1,220E+03	1,068E+03
4,840E+03	3,377E+03	2,956E+03	2,667E+03	1,861E+03	1,629E+03
5,744E+03	4,008E+03	3,510E+03	3,686E+03	2,572E+03	2,252E+03
8,712E+03	6,079E+03	5,330E+03	5,432E+03	3,790E+03	3,323E+03
1,670E+04	1,165E+04	1,026E+04	9,384E+03	6,546E+03	5,765E+03
9,501E+03	6,630E+03	5,840E+03	4,299E+03	3,000E+03	2,643E+03
1,013E+03	7,068E+02	6,228E+02	3,552E+02	2,478E+02	2,184E+02
1,654E+03	1,154E+03	1,017E+03	1,226E+03	8,551E+02	7,536E+02
6,980E+02	4,870E+02	4,285E+02	4,441E+02	3,098E+02	2,726E+02
7,672E+01	5,354E+01	4,715E+01	4,294E+01	2,997E+01	2,639E+01
6,708E+01	4,681E+01	4,148E+01	3,940E+01	2,750E+01	2,437E+01
3,401E+01	2,373E+01	2,131E+01	1,917E+01	1,338E+01	1,201E+01
1,899E+01	1,325E+01	1,196E+01	1,236E+01	8,626E+00	7,786E+00
9,121E-01	6,365E-01	5,733E-01	6,782E-01	4,733E-01	4,263E-01
6,528E+00	4,555E+00	4,116E+00	4,481E+00	3,127E+00	2,826E+00
5,059E+00	3,530E+00	3,157E+00	3,415E+00	2,383E+00	2,131E+00
8,666E-01	6,047E-01	5,385E-01	6,346E-01	4,428E-01	3,943E-01
1,771E+00	1,236E+00	1,097E+00	1,257E+00	8,772E-01	7,785E-01
1,160E+00	8,091E-01	7,104E-01	8,831E-01	6,160E-01	5,408E-01
2,789E-01	1,946E-01	1,695E-01	2,199E-01	1,534E-01	1,336E-01
1,252E-01	8,734E-02	7,583E-02	9,284E-02	6,476E-02	5,623E-02
5,427E+04	3,786E+04	3,327E+04	3,023E+04	2,110E+04	1,853E+04
41,9	41,9	41,8	42,0	42,0	41,9
2,276E+06	1,588E+06	1,392E+06	1,270E+06	8,863E+05	7,771E+05
4,214E+04	2,940E+04	2,581E+04	2,421E+04	1,689E+04	1,483E+04
54,0	54,0	53,9	52,5	52,5	52,4
	CP-5		RTNS-II		
	50,7		290,0		

Table 3. Gamma Damage in Iron and Copper

Gamma Energy (MeV)	Gamma $\sigma_{\Delta E}$ (barnkeV)	Gamma Damage in Iron PWR Flux 3.5%@30y g/cm²s	4.0%@30y g/cm²s	3.5%@40y g/cm²s	BWR Flux 45MWd@30y g/cm²s	45mWd@40y g/cm²s	40MWd@30y g/cm²s
9,500	6,097E-01						
7,000	3,808E-01						
5,000	2,217E-01						
3,500	1,204E-01						
2,750	7,736E-02						
2,250	5,170E-02			No data in this format			
1,750	2,911E-02						
1,250	9,935E-03						
0,850	1,919E-03						
0,575	1,004E-04						

Total Flux (g/cm²s)

Total $\sigma_{\Delta E}$ (barnkeV)

DE Rate (E-21eV/s)

Gamma Energy (MeV)	Gamma $s_{\Delta E}$ (barnkeV)	Gamma Damage in Copper PWR Flux @ Position A 3.5% @ 30y g/cm²s	4.0% @ 30y g/cm²s	3.5% @ 40y g/cm²s	BWR Flux @ Position A 45MWd@30y g/cm²s	45MWd@40y g/cm²s	40MWd@30y g/cm²s
9,500	4,828E-01	1,083E-01	8,467E-02	7,334E-02	8,550E-02	5,190E-02	5,219E-02
7,000	3,017E-01	1,194E+00	9,332E-01	8,039E-01	9,479E-01	6,572E-01	5,673E-01
5,000	1,838E-01	1,099E+01	8,580E+00	7,351E+00	8,545E+00	5,931E+00	5,217E+00
3,500	9,458E-02	2,488E+01	1,946E+01	1,687E+01	1,933E+01	1,340E+01	1,172E+01
2,750	6,037E-02	2,978E+01	3,005E+01	2,565E+01	2,129E+02	1,894E+02	1,687E+02
2,250	4,003E-02	4,091E+01	3,522E+01	2,817E+01	3,289E+01	2,338E+01	2,375E+01
1,750	2,209E-02	1,879E+05	1,912E+05	9,656E+04	1,730E+05	9,193E+04	1,497E+05
1,250	7,604E-03	2,708E+06	2,731E+06	1,246E+06	2,407E+06	1,144E+06	2,068E+06
0,850	1,025E-03	8,630E+05	8,777E+05	4,680E+05	7,493E+05	4,068E+05	6,558E+05
0,575	5,432E-05	1,457E+07	1,457E+07	1,231E+07	1,429E+07	1,133E+07	1,261E+07
Total Flux (g/cm²s)		1,833E+07	1,837E+07	1,412E+07	1,762E+07	1,297E+07	1,548E+07
Total $\sigma_{\Delta E}$ (barnkeV)		1,442E-03	1,453E-03	9,038E-04	1,344E-03	9,078E-04	1,318E-03
DE Rate (E-21eV/s)		2,643E+04	2,669E+04	1,276E+04	2,369E+04	1,178E+04	2,041E+04

Table 3. continue

Gamma Group Energy (MeV) Upper	Lower	Group $\sigma_{\Delta E}$ (barnkeV)	BWR Flux (38MWd@30y) Position D n/cm²s	Position I n/cm²s
6,000	5,000	2,600E-01	0,000E+00	0,000E+00
5,000	4,500	2,034E-01	0,000E+00	0,000E+00
4,500	4,000	1,685E-01	0,000E+00	0,000E+00
4,000	3,500	1,359E-01	0,000E+00	0,000E+00
3,500	3,000	1,055E-01	0,000E+00	0,000E+00
3,000	2,500	7,736E-02	0,000E+00	0,000E+00
2,500	2,000	5,170E-02	0,000E+00	0,000E+00
2,000	1,660	3,255E-02	2,792E+07	2,116E+06
1,660	1,500	2,264E-02	0,000E+00	0,000E+00
1,500	0,800	7,962E-03	5,569E+08	3,882E+07
0,800	0,510	2,910E-04	1,687E+10	6,353E+08
Total Flux (g/cm²s)			1,745E+10	6,762E+08
Total s_{DE} (barnkeV)			5,873E-04	8,323E-04
DE Rate (E-21eV/s)			1,025E+07	5,628E+05

Gamma Group Energy (MeV) Upper	Lower	Group $\sigma_{\Delta E}$ (barnkeV)	BWR Flux (38MWd @ 30y) Position I g/cm²s	Position A g/cm²s
6,000	5,000	2,198E+00	0,000E+00	0,000E+00
5,000	4,500	1,670E-01	0,000E+00	0,000E+00
4,500	4,000	1,357E-01	0,000E+00	0,000E+00
4,000	3,500	1,075E-01	0,000E+00	0,000E+00
3,500	3,000	8,240E-02	0,000E+00	0,000E+00
3,000	2,500	6,037E-02	0,000E+00	0,000E+00
2,500	2,000	4,003E-02	0,000E+00	0,000E+00
2,000	1,660	2,478E-02	2,116E+06	1,522E+05
1,660	1,500	1,664E-02	0,000E+00	0,000E+00
1,500	0,800	5,416E-03	3,882E+07	2,567E+06
0,800	0,510	1,202E-04	6,353E+08	2,270E+07
Total Flux (g/cm²s)			6,762E+08	2,542E+07
Total $s_{\Delta E}$ (barnkeV)			5,014E-04	8,027E-04
DE Rate (E-21eV/s)			3,391E+05	2,041E+04

3 Results

Displacement Rates After 30 Years Decay

For ease of comparison with the literature, the displacement rates for both neutrons and gammas will be calculated in the standard model /1/ with E_A = 40 eV for both Cu and Fe. This was the value used in calculating the efficiencies plotted in Figures (1) and (2). However, for neutrons, we need to keep in mind that the actual displacements for Fe are 1/2 this value and for Cu are 1/3. For electrons, the varying efficiencies are already included in the calculated damage energy rates.

For neutrons in copper (Table 1), the damage energy rates vary from 4 x 10^{-16} eV/s (BWR 40 MWd) to 9 x 10^{-16} eV/s (PWR 3.5%) at Position A. At the interface (I), rates vary from 8 x 10^{-16} eV/s (BWR 40 MWd) to 16 x 10^{-16} eV/s (PWR 3.5%). For gammas (Table 3) in copper, rates range from 2 x 10^{-17} eV/s (BWR 38 and 40 MWd) to 2.6 x 10^{-17} eV/s (PWR 3.5%) at A and 3.4 x 10^{-16} eV/s (BWR 38 MWd) to ~ 4.4 x 10^{-16} eV/s at I (estimated PWR 3.5%).

To convert to standard dpa rates/year (a more appropriate unit) we have for copper a maximum dpa rate at I of 5.0 x 10^{-10} dpa/year from neutrons and 1.7 x 10^{-10} dpa/year from gammas. Thus, initially about 25% of displacements are produced by gammas at position I.

Proceeding similarly for iron, we find the maximum and minimum rates at each position for the same cases as in copper. This gives a maximum dpa/year rate at D (Table 2) of 9.2 x 10^{-10} dpa/year from neutrons and 4.0 x 10^{-9} dpa/year from gammas. Thus, initially 80% of displacements are produced by gammas.

Damage Accumulations

If we were dealing with ordinary time scales, we could immediately dismiss the possibility of any materials radiation effects. However, for the spent fuel canisters we must consider times up to 100,000 years. If the rates above persisted for the entire time, we could expect measurable, but not necessarily compromising, radiation effects in both iron and copper. The accumulated damage, however, is significantly reduced by both the further decay of the source of the radiation and thermal annealing as the damage is produced.

Håkansson has calculated neutron and gamma dose rates for a BWR assembly as a function of time from 1 to 3x10^5 years. Results were given at 38 MWd/22/ and 55 MWd/23/ burn-ups. For neutrons dose rates are directly proportional to damage rates. Since the neutrons are produced by spontaneous fission or a-oxygen interactions in the fuel, neither spectra vary significantly with actinide species.

The tabulation below gives the initial damage rates in dpa/year and the accumulated neutron dpa for a BWR assembly (38–40 MWd) up to 100,000 years for iron (positions D and I) and copper (positions I and A). From the available data for a PWR assembly (50 MWd) we expect higher damage accumulations by a factor of 1.3. Although the initial rate for the PWR is 2.3 times greater, damage accumulations after 10,000 years are reduced /23/.

For the gammas the relation between dose rate and damage rate is more complicated since the spectra are changing with time. For example, in Table 3 for copper, the damage rate after 40 years decay is ~50% of that after 30 years for both BWR and PWR configurations, while dose rate is lowered to ~75% over the same period. From /21/ we can infer damage rates from dose rates by taking into account the half-lives of the contributing isotopes /24/.

If we define the initial ratio at 30 years as 1.00, at position A, we find it drops to .71 at 40 years, 0.54 at 50 and 0.34 at 100 years. It then rises to .38 at 300 and to a maximum of 2.34 at 1,000, drops to 2.10 at 10,000 years and continues dropping to 1.10 at 100,000 years. On this basis, gamma damage accumulations are also included below. In the PWR (50 MWd) case we again expect an increase by a factor of 1.3.

Initial Rates and Accumulations for a BWR Assembly (38–40 MWd)		Iron At D	Iron At I	Iron At I	Copper At	Copper A
Initial Damage Rates (10^{-10}dpa/year):	From neutrons	4.39	2.45		2.44	1.27
	From gammas	32.29	1.77		1.07	0.08
Damage at 10^5 Years (10^{-7} dpa):	From neutrons	5.79	3.23		3.22	1.68
	From gammas	1.50	0.07		0.04	.003

Thermal annealing effects will be included below in the discussion of property changes.

4 Discussion

From the above, using the factor 1.3 for both neutrons and gammas, the total maximum damage for copper at 100,000 years (4.2 x 10^{-7} dpa) will occur at position I for the PWR assembly with 1.2% from gammas. On the same basis, for iron at position D we expect 9.5 x 10^{-7} dpa with 16% from gammas. At less than 10^{-6} dpa, we would be hard-pressed to measure changes in any material property for room temperature irradiations with the possible exception of disordering of ordered alloys. Even in this case, the experimental resolution is only of the order of10^{-7} dpa /25/.

Mechanical Properties

For copper at 90°C at low doses, Heinisch and Martinez /26/ found an initial rate of change of the yield stress of 1Mpa/10^{-5} dpa in polycrystal, MARZ 5–9's grade material. With an initial yield stress of 60 MPa, it is comparable to that in the canister design /16/. Earlier work by Makin /27/ reported a similar rate of change for polycrystal copper with an initial yield of 35 MPa.

For iron at low doses, in high-purity single crystals, Aono et al /28/ found an abrupt rise in yield of 5MPa (25% of initial value) at 9 x 10^{-6}dpa, during neutron irradiation at 60C. Diehl et al /29/ reported an increase of 2MPa at an estimated dose of 3 x 10^{-6} dpa at 130C, again in a single crystal, but with 3–20 wtppm N. For polycrystals, Kinoshita et al /30/ found no changes until 3 x 10^{-4}dpa at room temperature, while Diehl et al /29/ reported in both single and polycrystal samples containing 100–200 wtppm N an abrupt increase from an initial yield of 50 to 85MPa at a dose of 9 x 10^{-6} dpa.

For both copper and iron, without any allowance for annealing, the accumulated dpa are at least an order of magnitude below those required for minimal changes in mechanical properties.

Radiation Enhanced Transport

Transport of impurities in materials by irradiation produced defects can have important effects on materials response. For neutron irradiation a maximum of 10–25% of the defects are free, i.e. they escape the initial event /8/. For gamma irradiation at room temperature nearly 100% survive to participate in transport. At 100C, in both iron and copper, both interstitials and vacancies are mobile. As a result, even at position D, all the defects will have reached their sinks before another damage event.

For both metals, the diffusion of free interstitials will provide some transport above that due to equilibrium processes. Because the maximum number produced (0.3ppm in iron and 0.08 ppm in copper) is much smaller than the concentration of any impurity already present /15/ and to transport any impurity it must first encounter that impurity, negligible redistribution will occur. The primary role of free interstitials will be to shrink or grow the clustered defects directly produced in the cascades and to a lesser extent modify existing impurity clusters.

For free vacancies in copper we do not expect any enhancement of segregation processes. The equilibrium vacancy concentration at 100C is 8×10^{-17} /31/ and the vacancy lifetime /32/ is ~1 second if we assume a typical dislocation density of 10^8 /cm^2. This will produce a flux of vacancies to sinks equal to the total free vacancies produced (8×10^{-8} over 10^5 years at position I) in only 30 years. Even the initial free vacancy production rate of 5×10^{-18} /s will produce a transient flux of only 6% of the equilibrium flux. At 10^5 years only 3×10^{-4} of the total vacancy flux to sinks arises from damage production.

In iron we can expect some enhancement of solute segregation for those impurities which diffuse through a vacancy method. The equilibrium vacancy concentration is 2×10^{-21} at 100C /33/ with a lifetime of~10^{-2} seconds. At this concentration it would take 10^4 years to produce the total free vacancy flux of 3×10^{-7} at position D. Thus, in 10^5 years, 9% of the vacancy flux to sinks is the result of damage production. However, because of the high vacancy formation energy (1.6 eV) this enhanced flux will be equivalent to 3×10^{-4} of the equilibrium flux at only 125°C. Because of the lower thermal conductivity of nodular cast iron compared to high purity copper, initially, we expect the temperature at D to be higher than the limit of 100°C /16/ at the surface of the canister. If it is as high or higher than 125°C, enhanced segregation effects will be negligible as above for copper.

5 Conclusions

By comparing with experiments in the literature, we were able to conclude that the magnitude of any physical property changes (e. g. yield stress, creep rates, enhanced solute segregation, dimensional changes, or brittleness) resulting from exposure to neutron and gamma radiation over the service life of the of the canister will be negligible. Therefore, materials radiation effects will not impose any additional constraints on canister design.

References

/1/ **Norgett M J, Robinson M T, Torrens I M, 1975.** Nucl Eng Des 33, 50.

/2/ **Kinchin G H, Pease R S, 1955.** Rep Prog Phys 18, 1.

/3/ **Kinney J H, Guinan M W, Munir Z A, 1984.** J Nucl Mater 122–123, 1028.

/4/ **Guinan M W, Abe H et al, unpublished 1987.**

/5/ **Simons R L, 1986.** J Nucl Mater 141–143, 665.

/6/ **Guinan M W, Kinney J H, 1981.** J Nucl Mater 103–104, 1319.

/7/ **Diaz de la Rubia T, Guinan M W, 1992.** Mater Res Forum 97/99, 23.

/8/ **R. S. Averback R S, Diaz de la Rubia T, 1998.** Solid State Physics, Vol 51, ed H Ehrenreich and D Turnbull, Academic Press, San Diego, p 281

/9/ **Håkansson R, 1994.** Studvik Nuclear Work Report-Technical Note (N(R)-94/038.

/10/ **Greenwood L R, Smither R K, 1985.** SPECTER: Neutron Damage Calculations for Materials Irradiations, Argonne National Laboratory, (ANL/FPP/TM-197.

/11/ Evaluated Nuclear Data File, National Neutron Cross Section Center, Brookhaven National Laboratory, Version ENDF/B-V, 1979.

/12/ **C. E. Klabunde C E, Coltman R R Jr, 1982.** J Nucl Mater 108–109,183.

/13/ **Wallner G, Anand M S, Greenwood L R, Kirk M A, Mansel W, Waschkowski W, 1988.** J Nucl Mater 152, 146.

/14/ **Kirk M A, Greenwood L R, 1979.** J Nucl Mater 80, 159.

/15/ Experimenters Guide, Rotating Target Neutron Source II Facility, Lawrence Livermore National Laboratory Internal Report M-094, July 1978.

/16/ **Werme L, 1998.**
SKB TR-98-08, Svensk Kärnbränslehantering AB

/17/ **Kinney J H, 1988.** DISP: Damage Energy Cross Section Calculations for Relativistic Electron Irradiations, Lawrence Livermore National Laboratory, unpublished.

/18/ **Bichsel H, 1972.** "Passage of Charged Particles Through Matter", in American Institute of Physics Handbook, 3rd Edition, D E Gray, Ed (McGraw-Hill, New York, 1972), Chap 8, p 142–189.

/19/ **Evans R D.** "Gamma Rays", ibid, Cha. 8, p 190–218.

/20/ **Cullen D E et al, 1989.** Tables and Graphs of Photon-Interaction Cross Sections from 10 eV to 100 GeV Derived from the LLNL Evaluated Photon Data Library (EPDL), Lawrence Livermore National Laboratory, (UCRL-50400-Vol.6-Pt A.

/21/ **Lundgren K, 1998.** Alara Engineering Report 97-028R Rev 1.

/22/ **Håkansson R, 1996.** Studvik Nuclear Work Report (N(R)-96/079, December,1996), (Note: the figure uses a dose rate scale of 100 per decade of graph requiring that interpolated mantissas be squared), Fig 15.

/23/ Ibid, Fig 16.

/24/ **Holden N E, 2001.** "Table of the Isotopes", in Handbook of Chemistry and Physics, 81st Edition, D. R. Lide, Ed. (CRC Press, New York, 2000/2001) Chap11, p 50–158.

/25/ **Huang J S, Guinan M W, Hahn P A, 1986.** J Nucl Mater 141–143, 888.

/26/ **Heinishe H L, Martinez C, 1986.** J Nucl Mater 141–143, 883.

/27/ **Makin M J, 1967.** in Radiation Effects, W. F. Sheely, Ed. Gordon and Breach, New York, p 627.

/28/ **Aono Y, Kuramoto E, Yoshida N, 1988.** J Nucl Mater 155–157, 1164.

/29/ **Diehl J, Merbold U, Reimold O, Weller M, 1973.** In Nuclear Metallurgy, Vol 18, R J Arsenault, Ed, National Bureau of Standards, Gaithersburg, p 69.

/30/ **Kinoshita K, Aono Y, Kuramoto E, Abe K, 1988.** J Nucl Mater 155–157, 893.

/31/ **Siegel R W, 1978.** J Nucl Mater 69–70, 117.

/32/ **Ehrhart P, Robock K H, Schober H R, 1986.** In Physics of Radiation Effects in Crystals, R. A. Johnson and A. N. Orlov, Eds. North-Holland, Amsterdam p 3.

/33/ **Schaefer H E, Maier K, Welter M, Herlach D, Seeger A, Diehl J, 1977.** Scr. Metal. 11, 803.